Title

Generating high-contrast, near single-cycle waveforms with third-order dispersion compensation.

Journal

Optics Letters, 42(4)

ISSN

0146-9592

Authors

Timmers, Henry
Kobayashi, Yuki
Chang, Kristina F
et al.

Publication Date

2017-02-15

DOI

10.1364/ol.42.000811

Peer reviewed

Optics Letters

Generating high-contrast, near single-cycle waveforms with third-order dispersion compensation

Henry Timmers,[1,4] Yuki Kobayashi,[1] Kristina F. Chang,[1] Maurizio Reduzzi,[1] Daniel M. Neumark,[1,2] and Stephen R. Leone[1,2,3,*]

[1]Department of Chemistry, University of California, Berkeley, California 94720, USA
[2]Chemical Sciences Division, Lawrence Berkeley National Laboratory, Berkeley, California 94720, USA
[3]Department of Physics, University of California, Berkeley, California 94720, USA
[4]e-mail: htimmers@berkeley.edu
*Corresponding author: srl@berkeley.edu

Received 21 November 2016; revised 25 January 2017; accepted 27 January 2017; posted 27 January 2017 (Doc. ID 281207); published 13 February 2017

Femtosecond laser pulses lasting only a few optical periods hold the potential for probing and manipulating the electronic degrees of freedom within matter. However, the generation of high-contrast, few-cycle pulses in the high power limit still remains nontrivial. In this Letter, we present the application of ammonium dihydrogen phosphate (ADP) as an optical medium for compensating for the higher-order dispersion of a carrier-envelope stable few-cycle waveform centered at 735 nm. The ADP crystal is capable of removing the residual third-order dispersion present in the spectral phase of an input pulse, resulting in near-transform-limited 2.9 fs pulses lasting only 1.2 optical cycles in duration. By utilizing these high-contrast, few-cycle pulses for high-harmonic generation, we are able to produce nanojoule-scale, isolated attosecond pulses.

OCIS codes: (320.7150) Ultrafast spectroscopy; (320.7110) Ultrafast nonlinear optics; (340.7480) X-rays, soft x-rays, extreme ultraviolet (EUV).

https://doi.org/10.1364/OL.42.000811

The application of intense laser pulses lasting only a few optical periods has revolutionized the field of ultrafast laser science. These so-called few-cycle pulses form the basis of attosecond science, enabling the isolation of single attosecond, extreme ultraviolet (XUV) pulses through the process of high-harmonic generation (HHG) [1]. In addition, few-cycle pulses can be used for the acceleration of electrons to MeV levels by laser-induced wakefield acceleration [2], imaging molecular structure via laser induced-electron diffraction [3], nanoscale imaging by photoemission electron microscopy [4], and nanoscale control by near-field enhancement in dielectric nanoparticles [5]. Few-cycle pulses approaching and surpassing the single cycle limit also present the prospect of probing the electronic degrees of freedom [6] within atoms [7], molecules [8], and even solid-state systems [9].

The generation of few-cycle pulses is typically accomplished through nonlinear broadening in a noble gas filled, hollow core fiber (HCF) [10,11]. A long fiber length guarantees sufficient nonlinear interaction with the gas medium to broaden the pulse spectrum up to an octave in bandwidth, while the high ionization potential of the noble gas helps to prevent detrimental plasma contributions. The nonlinear broadening imparts positive dispersion onto the output pulse, and subsequent dispersion compensation is required. This is generally accomplished by using a system of chirped multilayer mirrors [12] that impart negative effective dispersion and compensate for the intrinsic positive dispersion of the broadened pulse, as well as the positive dispersion introduced by additional experimental optics down the line. Chirped multilayer mirrors are typically engineered to compensate for some target or material phase. However, in practice, the chirped mirrors are typically employed to compensate for the second-order term in the Taylor expansion of the spectral phase. This second-order term is referred to as group-delay dispersion (GDD) and gives rise to the strongest contribution to the induced spectral phase of the broadened pulse. However, when driving HCF compression with high-energy pulses in the multi-millijoule regime, higher-order phase contributions can become significant, arising from processes such as self-steepening, ionization, and nonlinear mode coupling [13–15]. Therefore, higher-order phase compensation is necessary to achieve shorter pulses.

In this Letter, we introduce ammonium dihydrogen phosphate (ADP) as a material that helps to compensate for residual third-order dispersion (TOD) in a HCF-compressed few-cycle laser pulse. The integration of ADP in higher-order dispersion management allows for the production of intense, near-transform-limited and near single-cycle femtosecond pulses. These pulses can further be implemented to generate nanojoule-scale single attosecond pulses in Ar and Ne HHG media.

To generate near single-cycle waveforms, we begin with 1.8 mJ, 27 fs near-infrared (NIR) pulses from the output of a carrier-envelope phase stable Ti:sapphire amplifier. The pulses

are focused into a 1.5 m stretched HCF (Few-Cycle, Inc.) with an inner diameter of 400 μm. The fiber is statically filled with >2 bar of Ne gas to achieve an NIR spectral bandwidth $\Delta\lambda >$ 300 nm. The transmission through the gas-filled fiber results in a pulse energy of 0.95 mJ. The spectrally broadened pulses are then compressed using five pairs of double-angle, chirped multilayer mirrors (PC70, Ultrafast Innovations). Finally, the few-cycle waveforms are characterized with a D-scan module [16] (Sphere Ultrafast Photonics). In a D-scan measurement, the second-harmonic spectrum generated from the interaction of the few-cycle pulse with a thin BBO crystal is monitored as a function of dispersion (or glass insertion), yielding a frequency cross-correlation trace. The trace is then processed with a phase retrieval algorithm to uniquely characterize the few-cycle waveform [17].

In the absence of any additional dispersion compensation (i.e., only fused silica optics are placed into the beam path), we measure the D-scan trace presented in Fig. 1(a). The reconstructed spectral phase and intensity profile are plotted in Figs. 1(c) and 1(d) [red curves], respectively, corresponding to a reconstruction error [17] of 1.6%. From the D-scan measurement, it is already apparent that there is significant TOD in the pulse that appears as a tilt in the D-scan trace. From the reconstructed spectral phase, the amount of TOD is found to be ≈ – 100 fs^3, giving rise to a significant satellite structure in the intensity profile of the pulse.

Since the chirped mirrors are primarily used to compensate for GDD, optics demonstrating a ratio $r = \mathrm{TOD}/\mathrm{GDD} > 1$ fs can be used to compensate for the residual negative TOD in conjunction with the chirped mirror compressor.

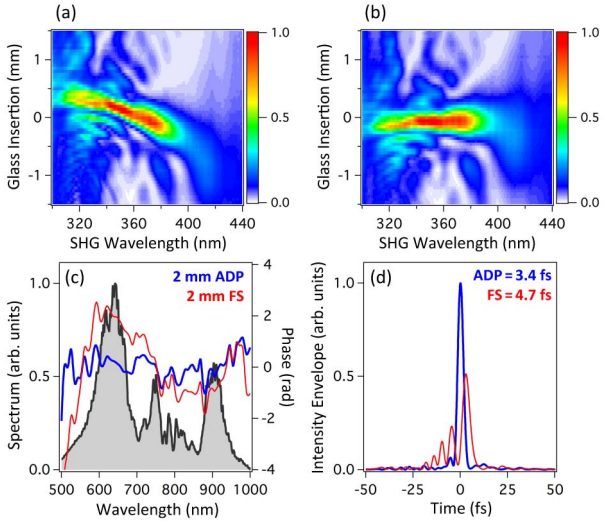

Fig. 1. (a) D-scan measurement of a few-cycle pulse compressed with only fused silica (FS) optics in the beam line. The tilt in the D-Scan trace is indicative of residual TOD. (b) D-scan measurement with 2 mm of ADP added into the beam line in place of 2 mm of fused silica. The resulting D-scan trace exhibits a flat profile, suggesting that the TOD has been removed. (c) Spectrum of the few-cycle waveform overlaid with the spectral phase reconstructions from D-scan traces (a) red curve and (b) blue curve. The obvious TOD measured in the fused silica spectral phase is removed with the addition of the ADP crystal. (d) Residual negative TOD imparts clear satellite pulses onto the reconstructed intensity envelope (red curve), broadening the pulse duration to 4.7 fs. High-contrast 3.4 fs pulses are measured when the ADP crystal is implemented to compensate for this residual TOD (blue curve).

Unfortunately, most crystals and windows exhibit $r < 1$ fs in the wavelength regime of the Ti:sapphire laser. In a previous report [16], Silva *et al.* found that water exhibited a value of $r >$ 1 fs (i.e., TOD ∼ 33 fs^3/mm and GDD ∼ 25 fs^2/mm) at a central wavelength of 800 nm and could be used to compensate for the residual negative TOD of the HCF-compressed pulse. However, due to the small ratio of TOD to GDD, a water cell of considerable thickness was required to compensate for the residual TOD which further necessitated additional chirped mirrors to compensate for the GDD introduced by the water and water cell windows. In this Letter, we utilize the fact that the ordinary axis of ADP exhibits a considerably higher TOD to GDD ratio (i.e., TOD ∼ 55 fs^3/mm and GDD ∼ 29 fs^2/mm). Furthermore, given that ADP has a smaller GDD than fused silica (GDD ≈ 36 fs^2/mm), ADP can be used to easily replace fused silica in the few-cycle beam path. A recent report [18] demonstrated that potassium dihydrogen phosphate also exhibits this advantageous property, but to a lesser extent.

The origin of the high TOD value for both water and ADP can be traced back to the strong absorption features that both materials exhibit in the mid-infrared (mid-IR) spectrum. These features give rise to anomalous dispersion, which amplifies the TOD component of the spectral phase in the NIR portion of the spectrum. Water exhibits a strong mid-IR feature at 3.1 μm due to a collection of OH-stretch vibrational modes in the liquid phase [19]. Similarly, ADP exhibits a strong mid-IR feature at 3.2 μm, arising from a collection of coupled O – H…O stretch and ammonium vibrations [20].

Based on the reconstructed phase in Fig. 1(c), we calculated that we would need to add approximately 2 mm of z-axis cut ADP (United Crystals, Inc.), while removing a similar amount of fused silica to fully compensate for the residual TOD. Experimentally, the addition of 2 mm of ADP to the few-cycle beam path (and the removal of approximately 2 mm of fused silica) yields the D-scan trace presented in Fig. 1(b). With the implementation of the ADP crystal, the tilt is removed from the D-scan trace yielding a flat reconstructed phase [Fig. 1(c), blue] and a high-contrast intensity envelope [Fig. 1(d), blue] corresponding to a reconstruction error of 1.4%. The reconstructed pulse duration was measured to be 3.4 fs compared to the transform-limit duration of 3.27 fs. Finally, the transmission through the chirped mirror compressor is 86%, and the transmission through the ADP crystal is 88%, resulting in a working pulse energy of 0.72 mJ.

To achieve the intense, 3.4 fs pulse measured in Fig. 1, the HCF was statically filled with a neon pressure of 2.3 bar. With the application of the ADP crystal for high-order dispersion compensation, we can now drive the HCF at higher pressures without destroying the temporal quality of the output pulse. The shortest pulse measured was collected at a Ne pressure of 2.8 bar. The corresponding D-scan trace and spectrum are shown in Figs. 2(a) and 2(b), respectively. The spectrum spanned from 500–1000 nm and supported a transform-limited pulse duration of 2.85 fs. The reconstructed phase [Fig. 2(b), red curve] yields a pulse duration of 2.9 fs (1.6% reconstruction error), representing a near-transform-limited, 1.2 cycle pulse at 735 nm. The corresponding electric field for this 1.2 cycle waveform is shown in Fig. 2(c). In addition, the reconstructed intensity envelope is shown in Fig. 2(d) (black, shaded curve), along with the transform-limited intensity envelope (red, dashed curve). It is clear that the ADP-compressed pulse is nearly identical to the transform-limited pulse.

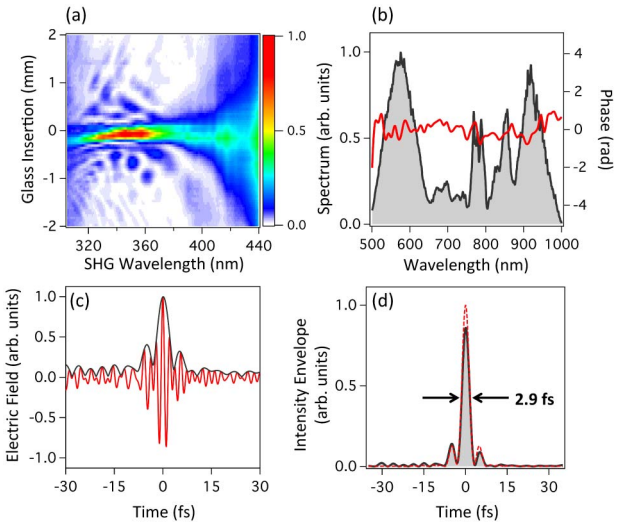

Fig. 2. (a) D-scan measurement for a few-cycle waveform generated with the hollow-core fiber statically filled to 2.8 bar of Ne. (b) Corresponding spectrum overlaid with the reconstructed spectral phase. The spectrum spans from 500 to 1000 nm and supports a transform-limited pulse duration of 2.85 fs. (c) Reconstructed electric field of the few-cycle waveform lasting only 1.2 optical cycles. (d) Reconstructed intensity envelope (black-shaded curve) exhibiting a pulse duration of 2.9 fs. The reconstructed envelope is nearly identical to the transform-limited envelope (red dashed curve).

To demonstrate the utility of these near single-cycle waveforms, we use the ADP-compressed pulses to isolate single attosecond pulses in Ar and Ne gas media. Due to the multi-cycle nature of laser fields, HHG inherently generates a train of attosecond pulses without active gating. Therefore, a sub-cycle gating technique must be incorporated to isolate a single attosecond pulse from the pulse train. Various gating schemes exist for isolating single attosecond pulses, the most popular including amplitude gating [21], polarization gating [22–24], and spatio-temporal gating [25]. The method of amplitude gating employs the use of few-cycle driving pulses for HHG emission. Since the electric field amplitude changes dramatically between each half-cycle, the highest energy XUV photons originate from high-harmonic emission at the most intense half-cycle, corresponding to the cutoff spectrum. By filtering this high-energy spectrum, one can obtain an isolated attosecond pulse. Polarization gating and spatio-temporal gating involve modification of the driving field by either imparting a time-dependent ellipticity or a spatio-temporal varying wavefront onto the field in order to isolate emission to a single half-cycle. As a result, the method of amplitude gating offers the potential of isolating the most intense attosecond pulses since the driving field remains unaltered. However, amplitude gating demands a very short driving pulse duration to achieve the necessary bandwidth for attosecond isolation. Pulse durations well below 4 fs are necessary for isolating high-contrast attosecond pulses in Ar and Ne gas media [24]. With the use of ADP-compressed waveforms, the demands of amplitude gating can easily be met.

To isolate an attosecond pulse in Ar, a 200 nm Al filter is first employed to remove the residual driving NIR field. We then take advantage of the Cooper minimum of Ar at 50 eV to isolate the higher energy cutoff spectrum from the lower energy harmonics [24,26]. By driving the HHG process with a 3.4 fs pulse, a broadband cutoff spectrum is generated which extends from the Cooper minimum at 50 eV to the aluminum edge at 72.6 eV. The corresponding spectrum for such an attosecond pulse isolated in Ar is shown in Fig. 3(a). The technique of attosecond streaking is used both to confirm the isolation of the attosecond pulse and to characterize the attosecond pulse duration. Briefly, energy-resolved photoelectrons ionized by the attosecond pulse in Ne gas are monitored as a function of a XUV-pump, NIR-probe time delay [27]. As the NIR field overlaps with the ionized photoelectrons, it imparts a delay-dependent momentum shift onto the photoelectron wavepacket. The resulting spectrogram can be processed with a two-dimensional phase retrieval algorithm to uniquely characterize the XUV and NIR fields. The experimentally measured attosecond streaking trace for the pulse isolated in Ar is shown in Fig. 3(b). The clean 1ω oscillation confirms the high contrast of the isolated attosecond pulse. We can further process the streaking spectrogram using a ptychographic reconstruction algorithm [28]. The reconstructed XUV phase is overlaid with the spectrum in Fig. 3(a), corresponding to a reconstruction error of 2.1%. The phase exhibits a slight positive chirp at higher energy due to the Al edge and reconstructs to a pulse duration of 170 as.

To isolate attosecond pulses in Ne, a 200 nm Zr filter is used both to filter out the residual NIR field and to isolate the cutoff spectrum. In addition, a micro-channel plate filter is placed before the Zr filter to attenuate the driving NIR field and prevent laser-induced damage of the Zr filter [29]. Figure 3(c) shows the XUV spectrum for a pulse isolated in Ne using the 3.4 fs, ADP-compressed waveform. Due to the broad bandwidth of the Zr filter, we can achieve a continuous spectrum spanning from 70 to 120 eV. The measured streaking trace for this pulse is shown in Fig. 3(d). While the trace demonstrates a strong 1ω oscillation, a weak satellite pulse can be seen at higher photoelectron energies which is out of phase with the main streaking trace. Since the bandwidth of the Zr filter

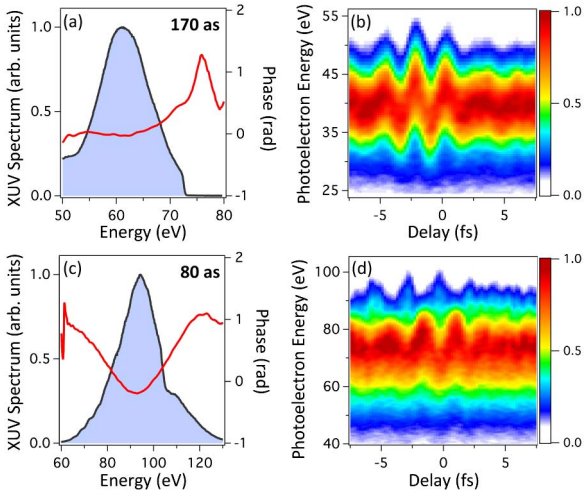

Fig. 3. (a) Attosecond XUV spectrum for a pulse isolated via amplitude gating in Ar using the ADP-compressed waveform. The reconstructed phase is overlaid with the spectrum resulting in a 170 as pulse duration. (b) Experimentally measured attosecond streaking trace used to reconstruct the phase of the Ar XUV pulse. (c) and (d) Similar to (a) and (b), except Ne is used as a HHG medium. The reconstructed pulse duration is measured to be 80 as. In addition, a clear out-of-phase streaking trace is measured in this spectrogram originating from a 5% satellite pulse contamination.

is so broad, isolating a single attosecond pulse at the cutoff is rather challenging. The high-energy satellite accounts for approximately 5% of the total spectrum and arises due to the emission from an adjacent half-cycle, which exhibits a greater recombination energy. The reconstructed XUV phase is overlaid with the spectrum in Fig. 3(c), corresponding to a reconstruction error of 2.2%. The phase exhibits a positive chirp, intrinsic to the HHG process, and reconstructs to a pulse duration of 80 as.

The pulse energy of the amplitude-gated, attosecond pulses can be estimated from the XUV response of the x-ray camera and the transmission of various optics in the beamline, both of which have been calibrated in a previous study [24]. From this estimation, we find that the pulse energies for the attosecond continua isolated in Ar and Ne are ≈1 nJ. It may be surprising that attosecond pulses isolated in Ne exhibit a similar pulse energy as those in Ar since the ionization potential of Ne is notably greater than that of Ar. However, due to the short pulse duration and high power of the ADP-compressed, few-cycle waveform, we are not intensity limited in the generation of attosecond pulses in either driving gas. As a result, the flux of the generated pulses is more dependent on the dipole recombination cross section. Since the dipole recombination cross section can be approximated using the photo-ionization cross section, we find that Ne exhibits a four-fold greater photo-ionization cross section than Ar in the energy range of the isolated attosecond pulses [30]. Therefore, the lower ionization probability due to the higher ionization potential of Ne is partially compensated by the greater dipole recombination cross section.

In conclusion, we have demonstrated the use of ADP in the higher-order dispersion management of a HCF-compressed, few-cycle waveform. The utilization of ADP in compensating the spectral TOD allows for the near-transform-limited compression of few-cycle pulses approaching the single-cycle limit. The application of these ADP-compressed waveforms in HHG allows for the production of nanojoule-scale isolated attosecond pulses between 50 and 120 eV. The production of such pulses could be scaled to perform a proper attosecond XUV-pump, XUV-probe-type experiment [31]. Moreover, the use of ADP-compressed, few-cycle waveforms in the strong field ionization of molecular targets could be used to generate and probe correlated, multi-electronic wavepackets [32].

Funding. Army Research Office (ARO) (W911NF-14- 1-0383); National Science Foundation (NSF) (CHE-1361226); Funai Overseas Scholarship.

Acknowledgment. H. Timmers and Y. Kobayashi were supported by ARO. K. Chang and M. Reduzzi were supported by the NSF. Y. Kobayashi additionally acknowledges financial support from the Funai Overseas Scholarship. The authors would like to thank Helder Crespo, Rosa Romero, and Francisco Silva from Sphere Ultrafast Photonics for their fruitful discussions on pulse compression, as well as Bruno Schmidt from Few-Cycle, Inc., for sharing his knowledge and experience on hollow-core fibers.

REFERENCES

1. M. Chini, K. Zhao, and Z. Chang, Nat. Photonics **8**, 178 (2014).
2. K. Schmid, L. Veisz, F. Tavella, S. Benavides, R. Tautz, D. Herrmann, A. Buck, B. Hidding, A. Marcinkevicius, U. Schramm, M. Geissler, J. M. ter Vehn, D. Habs, and F. Krausz, Phys. Rev. Lett. **102**, 124801 (2009).
3. M. G. Pullen, B. Wolter, A.-T. Le, M. Baudisch, M. Hemmer, A. Senftleben, C. D. Schröter, J. Ullrich, R. Moshammer, C. D. Lin, and J. Biegert, Nat. Commun. **6**, 7262 (2015).
4. E. Mårsell, A. Losquin, R. Svärd, M. Miranda, C. Guo, A. Harth, E. Lorek, J. Mauritsson, C. L. Arnold, H. Xu, A. L'Huillier, and A. Mikkelsen, Nano Lett. **15**, 6601 (2015).
5. S. Zherebtsov, T. Fennel, J. Plenge, E. Antonsson, I. Znakovskaya, A. Wirth, O. Herrwerth, F. S. Man, C. Peltz, I. Ahmed, S. A. Trushin, V. Pervak, S. Karsch, M. J. J. Vrakking, B. Langer, C. Graf, M. I. Stockman, F. Krausz, E. Rühl, and M. F. Kling, Nat. Phys. **7**, 656 (2011).
6. K. Ramasesha, S. R. Leone, and D. M. Neumark, Annu. Rev. Phys. Chem. **67**, 41 (2016).
7. E. Goulielmakis, Z. Loh, A. Wirth, R. Santra, N. Rohringer, V. Yakovlev, S. Zherebtsov, T. Pfeifer, A. Azzeer, M. Kling, S. Leone, and F. Krausz, Nature **466**, 739 (2010).
8. F. Calegari, D. Ayuso, L. Belshaw, S. D. Camillis, S. Anumula, F. Frassetto, L. Poletto, A. Palacios, P. Decleva, J. B. Greenwood, F. Martín, and M. Nisoli, Science **346**, 336 (2014).
9. M. Schultze, K. Ramasesha, C. D. Pemmaraju, S. A. Sato, D. Whitmore, A. Gandman, J. S. Prell, L. J. Borja, D. Prendergast, K. Yabana, D. M. Neumark, and S. R. Leone, Science **346**, 1348 (2014).
10. M. Nisoli, S. D. Silvestri, O. Svelto, R. Szipöcs, K. Ferencz, C. Spielmann, S. Sartania, and F. Krausz, Opt. Lett. **22**, 522 (1997).
11. T. Brabec and F. Krausz, Rev. Mod. Phys. **72**, 545 (2000).
12. V. Pervak, I. Ahmad, M. K. Trubetskov, A. V. Tikhonravov, and F. Krausz, Opt. Express **17**, 7943 (2009).
13. T. Balciunas, C. Fourcade-Dutin, G. Fan, T. Witting, A. A. Voronin, A. M. Zheltikov, F. Gerome, G. G. Paulus, A. Baltuska, and F. Benabid, Nat. Commun. **6**, 6117 (2015).
14. P. Béjot, B. E. Schmidt, J. Kasparian, J.-P. Wolf, and F. Legaré, Phys. Rev. A **81**, 063828 (2010).
15. M. Nurhuda, A. Suda, K. Midorikawa, M. Hatayama, and K. Nagasaka, J. Opt. Soc. Am. B **20**, 2002 (2003).
16. F. Silva, M. Miranda, B. Alonso, J. Rauschenberger, V. Pervak, and H. Crespo, Opt. Express **22**, 10181 (2014).
17. M. Miranda, C. L. Arnold, T. Fordell, F. Silva, B. Alonso, R. Weigand, A. L'Huillier, and H. Crespo, Opt. Express **20**, 18732 (2012).
18. M. Miranda, J. Penedones, C. Guo, A. Harth, M. Louisy, L. Neoricic, A. L'Huillier, and C. L. Arnold, "Generalized projection retrieval of dispersion scans for ultrashort pulse characterization," arXiv:1610.04502 (2016).
19. D. M. Carey and G. M. Korenowski, J. Chem. Phys. **108**, 2669 (1998).
20. H. Zhou, F. Wang, M. Xu, B. Liu, F. Liu, L. Zhang, X. Xu, X. Sun, and Z. Wang, J. Cryst. Growth **450**, 6 (2016).
21. E. Goulielmakis, M. Schultze, M. Hofstetter, V. S. Yakovlev, J. Gagnon, M. Uiberacker, A. L. Aquila, E. M. Gullikson, D. T. Attwood, R. Keinberger, F. Krausz, and U. Kleineberg, Science **320**, 1614 (2008).
22. I. J. Sola, E. Mével, L. Elouga, E. Constant, V. Strelkov, L. Poletto, P. Villoresi, E. Benedetti, J.-P. Caumes, S. Stagira, C. Vozzi, G. Sansone, and M. Nisoli, Nat. Phys. **2**, 319 (2006).
23. S. Gilbertson, H. Mashiko, C. Li, S. D. Khan, M. M. Skakya, E. Moon, and Z. Chang, Appl. Phys. Lett. **92**, 071109 (2008).
24. H. Timmers, M. Sabbar, J. Hellwagner, Y. Kobayashi, D. M. Neumark, and S. R. Leone, Optica **3**, 707 (2016).
25. K. T. Kim, C. Zhang, T. Ruchon, J.-F. Hergott, T. Auguste, D. M. Villeneuve, P. B. Corkum, and F. Quéré, Nat. Photonics **7**, 651 (2013).
26. H. J. Wörner, H. Niikura, J. B. Betrand, P. B. Corkum, and D. M. Villeneuve, Phys. Rev. Lett. **102**, 103901 (2009).
27. E. Goulielmakis, V. S. Yakovlev, A. L. Cavalieri, M. Uiberacker, V. Pervak, A. Apolonski, R. Kienberger, U. Kleineberg, and F. Krausz, Science **317**, 769 (2007).
28. M. Lucchini, M. H. Brügmann, A. Ludwig, L. Gallmann, U. Keller, and T. Feurer, Opt. Express **23**, 29502 (2015).
29. Q. Zhang, K. Zhao, J. Li, M. Chini, Y. Cheng, Y. Wu, E. Cunningham, and Z. Chang, Opt. Lett. **39**, 3670 (2014).
30. J. A. R. Samson and W. C. Stolte, J. Electron Spectrosc. **123**, 265 (2002).
31. E. J. Takahashi, P. Lan, O. D. Mücke, Y. Nabekawa, and K. Midorikawa, Nat. Commun. **4**, 2691 (2013).
32. A. I. Kuleff, J. Breidbach, and L. S. Cederbaum, J. Chem. Phys. **123**, 044111 (2005).